Journal of proteome research

pubs.acs.org/jpr

Article

Automated Spatially Targeted Optical Microproteomics Investigates Inflammatory Lesions *In Situ*

Bocheng Yin, Laura R. Caggiano, Rung-Chi Li, Emily McGowan, Jeffrey W. Holmes, and Sarah E. Ewald*

Cite This: *J. Proteome Res.* 2021, 20, 4543−4552

Read Online

ACCESS | Metrics & More | Article Recommendations | Supporting Information

ABSTRACT: Tissue microenvironment properties like blood flow, extracellular matrix, or proximity to immune-infiltrate are important regulators of cell biology. However, methods to study regional protein expression in the native tissue environment are limited. To address this need, we developed a novel approach to visualize, purify, and measure proteins *in situ* using automated spatially targeted optical microproteomics (AutoSTOMP). Here, we report custom codes to specify regions of heterogeneity in a tissue section and UV-biotinylate proteins within those regions. We have developed liquid chromatography−mass spectrometry (LC−MS)/MS-compatible biochemistry to purify those proteins and label-free quantification methodology to determine protein enrichment in target cell types or structures relative to nontarget regions in the same sample. These tools were applied to (a) identify inflammatory proteins expressed by $CD68^+$ macrophages in rat cardiac infarcts and (b) characterize inflammatory proteins enriched in $IgG4^+$ lesions in human esophageal tissues. These data indicate that AutoSTOMP is a flexible approach to determine regional protein expression *in situ* on a range of primary tissues and clinical biopsies where current tools and sample availability are limited.

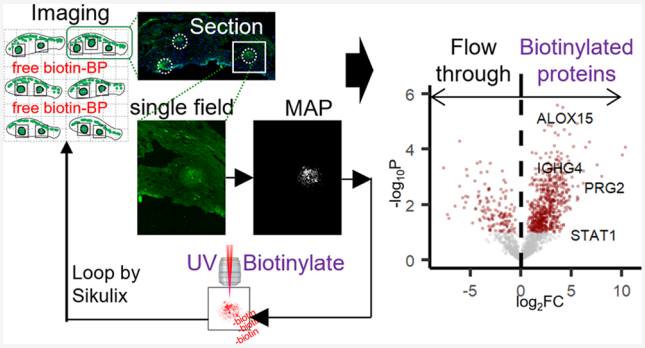

KEYWORDS: *AutoSTOMP, discovery proteomics, inflammation, proximity biotinylation*

INTRODUCTION

Technological advances and innovation in "big data" analysis tools have revolutionized the proteomics in the last decades. These tools are still most frequently applied to studying protein expression in isolated cell types or in bulk tissue lysates. There is still a tremendous need for discovery proteomics techniques designed to study the biology of specific cell types in the context of the *in situ* tissue microenvironment. Laser capture microdissection (LCM) can isolate individual cells down to ∼10 μm resolution for proteomics analysis.[1] However, this process is time-intensive and susceptible to neighboring cell contamination. More recently, mass spectrometric imaging approaches have facilitated protein discovery using matrix-assisted laser desorption/ionization (MALDI) of cells or cell *in situ* at a 50−100 μm scale.[2] This approach provides strong regional selectivity, but it is "qualitative" rather than "quantitative" because MALDI-mass spectrometry imaging (MSI) cannot directly identify the protein without adequate resolution for peptide fragment sequencing.[2−4] We recently developed a technique called automated spatially targeted optical microproteomics (AutoSTOMP), which uses standard immunofluorescence imaging to visualize structures of interest (SOI) and the two-photon laser source to selectively conjugate photoactivatable-biotin tags to any protein within the structure. Biotinylated proteins are then isolated by streptavidin (SA) precipitation and identification by liquid chromatography−mass spectrometry (LC−MS)/MS with label-free quantitation protocol. Previously, we demonstrated that AutoSTOMP enriches proteins from the obligate intracellular pathogen *Toxoplasma gondii* within infected human and mouse macrophages.[5] By modifying the MAP to encompass the region surrounding but excluding *T. gondii*, host and *T. gondii* proteins localized to the parasite vacuole membrane were identified. These studies demonstrated that AutoSTOMP can enrich proteins at a 1 μm scale and identify proteins with as little as 1 μg of protein per sample.[5] Proximity-based protein discovery tools that use a label-targeting enzyme to biotinylate nearby proteins (BioID, TurboID, APEX) have an excellent resolution of ∼10 nm.[6,7] However, they are limited to cell lines or animal models that have tools for genetic modification.

Received: June 18, 2021
Published: August 26, 2021

https://doi.org/10.1021/acs.jproteome.1c00505
J. Proteome Res. 2021, 20, 4543−4552

Alternatively, in SPPLAT/BAR, biotin targeting is mediated by antibodies conjugated to a peroxidase.[8,9] Image-guided tagging is a central advantage of AutoSTOMP, which allows the user to specify biotin targeting based on colocalization stains or by thresholding, dilating, or eroding the boundaries of the image used to guide biotinylation at least 10 times the resolution of laser capture microdissection.[1] Any sample where one or more fluorescent markers (e.g., tags, probes, or antibodies) are available to identify SOI is a candidate for AutoSTOMP, so this technique could be a transformative approach to perform localization-dependent protein discovery on a broad range of human clinical specimens.

In practice, however, adapting AutoSTOMP for tissue sections poses several unique challenges compared to that for cell culture samples. These include identifying signal versus background in tissues with high or variable autofluorescence, automating the selection of SOI within tissue microdomains rather than elsewhere in a section (particularly for low-density SOI), and optimizing the digestion and streptavidin precipitation biochemistry to handle fixed tissues with extensive extracellular matrix networks using a protocol compatible with LC−MS.[10] Here, we report the AutoSTOMP workflow to address the unique demands of *in situ* proteomics. This includes an updated software analysis package that defines the coordinates of multiple sections on a slide, identifies relevant microdomains of each section, and generates a tile array to automate SOI cross-linking. We have developed biochemistry protocols to examine protein enrichment in inflammatory lesions using two disease systems: (1) a rat cardiac infarct model, chosen as a tissue type with extensive extracellular matrix protein cross-linking, which poses a difficulty for protein purification; and (2) human eosinophilic esophagitis (EoE), selected for the small biopsy size and low frequency of lesions in each tissue section.

EXPERIMENTAL SECTION

Note: full protocols can be found in the Supplementary Methods section of the Supporting information.

Rat Cardiac Infarct and Eosinophilic Esophagitis (EoE) Biopsy Collection and Staining

Rat myocardial infarcts were induced in 8 week old male Sprague-Dawley rats (Envigo) by the left anterior descending (LAD) coronary artery permanent ligation. One week post surgery, the scar region was dissected, frozen in liquid-nitrogen-chilled isopentane, and embedded in OTC. Seven micrometer cryosections were methanol-fixed for 20 min on ice and stained with an antibody specific to CD68 (clone: ED1, Bio-Rad). Animal protocols were approved by the University of Virginia Institutional Animal Care and Use Committee.

Six 1 mm biopsies were collected from a patient diagnosed with active EoE (ε15 eosinophils/hpf), according to consensus guidelines, using standard endoscopy procedures.[11] Biopsies were fixed and sectioned as described and stained with an antibody specific to human immunoglobuin lgG4 (clone MRQ-44, Cell Marque). The human study was approved by the University of Virginia Institutional Review Board (IRB), which requires written participant consent (IRB-HSR#19562).

Tissue sections were treated with an avidin/biotin blocking kit (SP-2001, Vector Laboratories) and then mounted with biotin-dPEG3-benzophenone (Biotin-BP, Quanta BioDesign) in 50:50 (v/v) dimethyl sulfoxide (DMSO)/water at a concentration of 1 mM. Each slide was prepared immediately prior to AutoSTOMP imaging.

AutoSTOMP 2.0

Imaging and photo-cross-linking were performed on an LSM880 microscope (Carl Zeiss) equipped with a 25× oil immersion lens (LD LCI Plan-Apochromat 25×/0.8 Imm Korr DIC M27) and a Chameleon multiphoton light source (Coherent). AutoSTOMP 2.0, the upgraded SikuliX (version 1.1.4, http://sikulix.com/) integrated workflow, was modified from the previous protocol[5] and scripted for the tissue to facilitate SOI selection on multiple tissue sections per microscopic slide. Step-by-step instruction and source codes are deposited at https://github.com/boris2008/AutoSTOMP_2.0.git.

Following photolabeling, each sample was detached from the coverslip. Excess, unconjugated biotin-BP was rinsed with 50:50 (v/v) DMSO/water three times and then with water three times. The slides were stored at −80 °C before processing replicates in tandem. Rat cardiac sections were lysed in the hydroxylamine lysis buffer[10] (1 M NH_2OH−HCl, 8 M urea, 0.2 M K_2CO_3, pH = 9.0) at 45 °C for 17 h to extract proteins from the insoluble extracellular matrix. EoE biopsy sections were lysed in dithiothreitol/sodium dodecyl sulfate (DTT/SDS) buffer[12,13] (0.1 M Tris−HCl, 0.1 M DTT, 4% SDS, pH = 8.0) at 99 °C for 1 h. Tissue lysates were then diluted 1:10 in TBS-0.1% SDS and then incubated with streptavidin (SA) magnetic beads (Pierce #88817) at room temperature for 1 h. Biotinylated proteins were precipitated by a magnet. The unbound proteins were collected as the "flow-through" fraction and precipitated with 100% trichloroacetic acid. The biotinylated proteins were eluted from the magnetic beads in laemmli buffer at 96 °C for 5 min and collected as the AutoSTOMP fraction. The protein pellet of the flow-through fraction was resuspended in laemmli buffer at 96 °C for 5 min. The fractions were resolved in the sodium dodecyl sulfate-polyacrylamide gel electrophoresis (SDS-PAGE) gel at 70 V for 12 min. For each lane, a 1 cm gel fragment was excised and submitted for mass spectrometry analysis at the University of Virginia Biomolecular Analysis Facility. The samples were run on a Thermo Orbitrap Exploris 480 mass spectrometer system with an Easy Spray ion source connected to a Thermo 75 μm × 15 cm C18 Easy Spray column (trap column first). Six microliters of the extract was injected, and the peptides were eluted from the column by an acetonitrile/0.1 M formic acid gradient at a flow rate of 0.3 μL/min over 2.0 h. The nanospray ion source was operated at 1.9 kV. The digest was analyzed using the rapid switching capability of the instrument acquiring a full scan mass spectrum to determine peptide molecular weights followed by product ion spectra (Top10 HCD) to determine amino acid sequence in sequential scans.

The raw mass spectra data were parsed by MaxQuant[14] (versions 1.6.14.0, Max Planck Institute of Biochemistry). The MS raw and MaxQuant search data ($CD68^+$ data in Figure 2: accession: PXD026818; and EoE data in Figure 5: accession: PXD026819) have been deposited at PRIDE (https://www.ebi.ac.uk/pride/). The MaxQuant results were then analyzed following the label-free quantification (LFQ) data analysis protocol.[14] Student's *t* test (permutation-based FDR < 0.05) and T-distributed stochastic neighborhood embedding (t-SNE) clustering[15] were applied in Perseus[16] (versions 1.6.14.0, Max Planck Institute of Biochemistry). The resulting data were plotted in R (www.r-project.org) with the installed packages

https://doi.org/10.1021/acs.jproteome.1c00505
J. Proteome Res. 2021, 20, 4543−4552

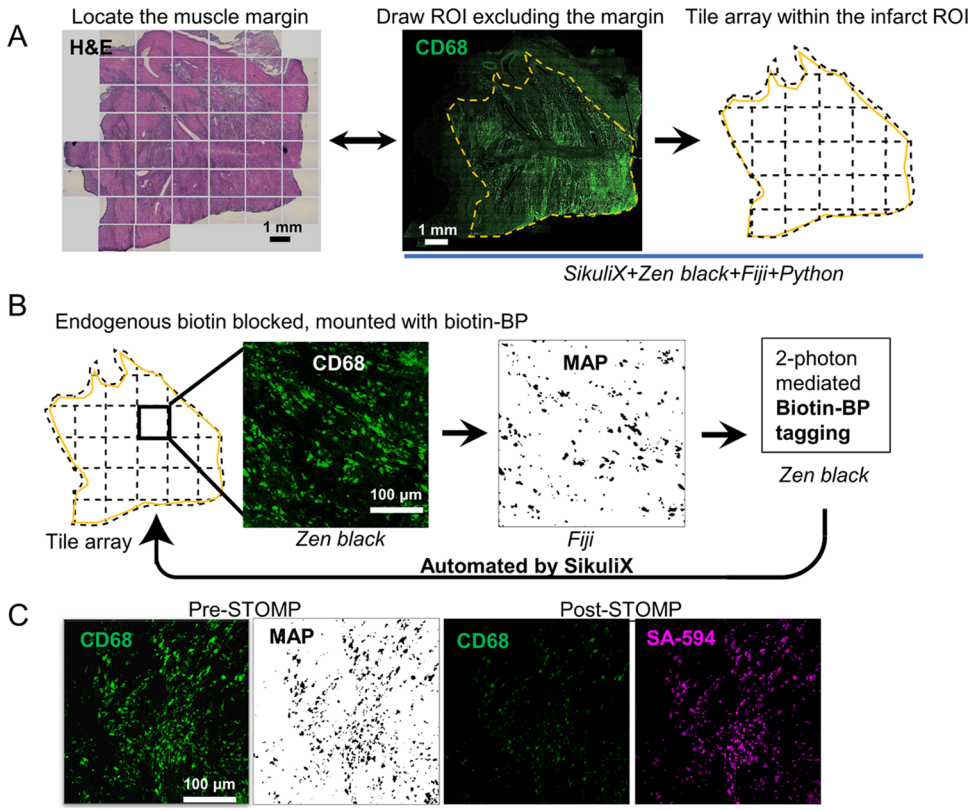

Figure 1. AutoSTOMP identifies rat cardiac infarct borders and biotinylates CD68-associated proteins in tissue sections. (A) Serial sections of cardiac infarcts were stained with hematoxylin and eosin (H&E, left) to identify the general border of the infarct relative to health tissues or the macrophage marker CD68 (green). Infarct borders were defined (yellow) and divided into tiles. (B) AutoSTOMP workflow integrates the jobs repeated in tiles. In Zeiss Zen Black, the CD68 signal is imaged on each tile, exported to FIJI where it is thresholded and used to generate an MAP file, identifying the pixel coordinates of the $CD68^{+}$-positive SOI. The MAP file is imported into Zen Black and directs the two-photon to target biotin-BP to the CD68+ SOI. This is automated across the scar. Each field of view measures 340 μm × 340 μm. A typical section contains approximately 550 tiles. (C) To validate the selective biotinylation of $CD68^{+}$ SOI (pre-STOMP), slides were washed, stained with streptavidin-594 and then reimaged (post-STOMP) to assess CD68 (note photobleaching) and streptavidin colocalization.

"ggplot2", "ggrepel", "heatmap.2", or using GraphPad Prism (version 8.2.1).

Immunofluorescence and Streptavidin Fluorescence Staining

To validate biotin-BP cross-linking, following AutoSTOMP 2.0 cross-linking, some samples were washed and stained with AlexaFluor-594 streptavidin (#016-580-084, Jackson ImmunoResearch) in TBST. Samples were reimaged to colocalize with the CD68 or lgG4 signal. For immunofluorescence costaining experiments, samples were fixed and sectioned as described for AutoSTOMP and then blocked in 5% bovine serum albumin (BSA) and 1:200 Fc block (human FC Clone 3070, BD or rodent FC block clone 93, Affymetrix) for 1 h in TBST prior to staining. A full list of antibodies for validation is provided in the Supporting Information.

RESULTS AND DISCUSSION

Cardiac Infarct Macrophages Are Selectively Biotinylated by AutoSTOMP

Automated spatially targeted optical microproteomics (AutoSTOMP)[5] is a proximity-based protein labeling tool that uses standard fluorescence microscopy to visualize structures of interest (SOI). The fluorescence signal is used to identify the pixel coordinates of the SOI and generate an MAP file. The MAP file then guides two-photon excitation of the SOI with UV energy light, which conjugates benzophenone-biotin (biotin-BP) present in the mounting media to any nearby carbon or nitrogen via the benzophenone moiety. Imaging, MAP generation, and biotin-BP conjugation are repeated for every field of view and automated using SikuliX icon recognition software. Once biotinylation is complete, unconjugated biotin-BP is washed away. The samples are digested off of the slide. Biotinylated proteins are streptavidin-precipitated and then digested for identification by liquid chromatography−mass spectrometry (LC−MS).[5]

To test the ability of the AutoSTOMP protocol to selectively biotinylate structures of interest within tissue sections, we first examined a rat myocardial infarction model. In this model, trauma caused by ligation and infiltrating immune cells causes fibroblast activation and deposition of scar tissues that ultimately impairs cardiac function. Macrophages are thought to play a role in inflammatory regulation and damaged cell turnover in the tissue. One week after surgical ligation on the left anterior descending (LAD) coronary artery, the infarct region was dissected and cryosectioned for immunofluorescence staining. The infarct region or scar is defined by loss of organized cardiac muscle structure, regions of extracellular matrix, and fibroblast expansion, as well as infiltrating immune cells. To differentiate between the scar and neighboring healthy tissue, low-resolution tile scans were performed on adjacent serial sections stained with hematoxylin

https://doi.org/10.1021/acs.jproteome.1c00505
J. Proteome Res. 2021, 20, 4543−4552

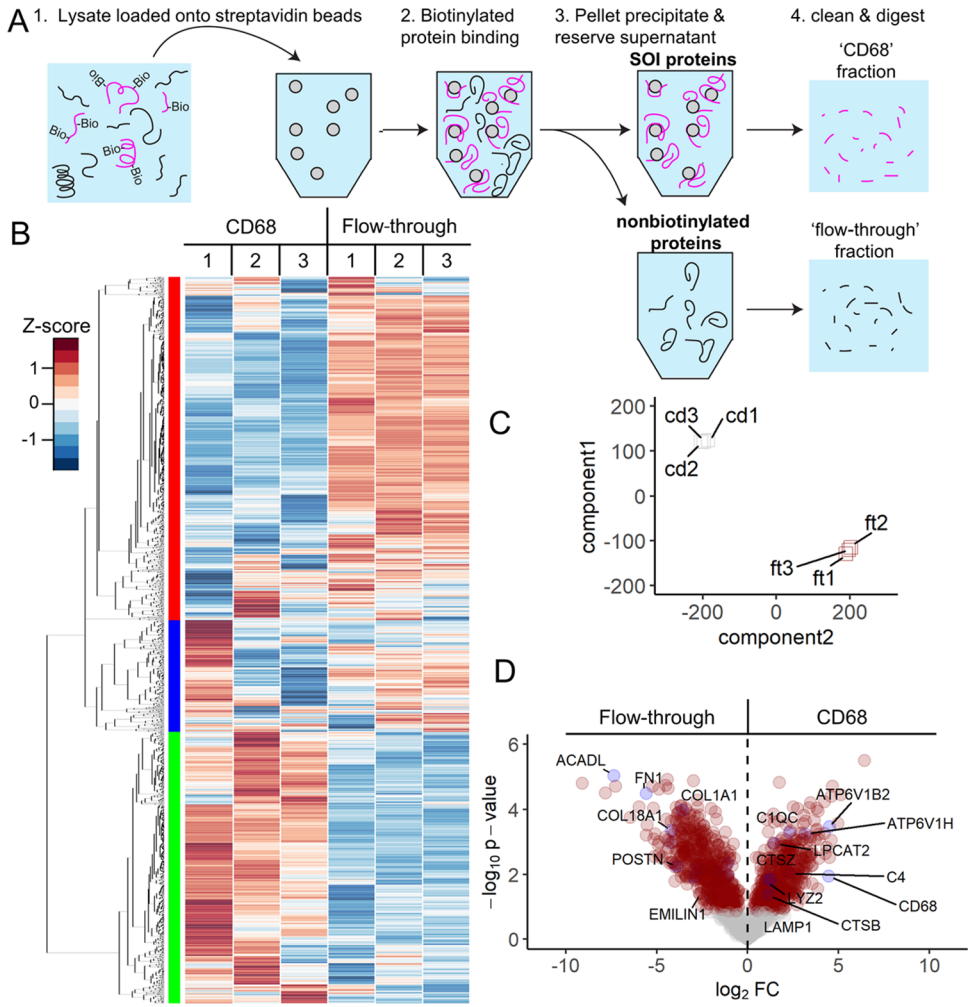

Figure 2. AutoSTOMP selectively enriches macrophage-associated proteins in the CD68$^+$ regions of rat cardiac infarcts. CD68$^+$ regions of the cardiac infarcts are biotinylated by AutoSTOMP, as described in Figure 1. (A) After AutoSTOMP cross-linking, coverslips were washed of unconjugated biotin-BP and lysed (1). Biotinylated proteins (CD68 fraction) were bound to streptavidin beads (2) and pelleted (3). Unbound proteins were reserved as a flow-through control (3). Both fractions are trypsin/LysC-digested and analyzed by LC−MS (4). (B−D) Protein abundance was determined by MaxQuant label-free quantification (MaxLFQ). (B) Of the 1671 rat proteins identified, 94.2% were observed with one or more valid readouts in each of the three CD68 and/or flow-through fraction replicates. Heatmap represents z-score for each protein across all of the samples. Hierarchical clustering (left) indicates three enrichment patterns. (C) T-distributed stochastic neighborhood embedding (t-SNE) analysis of variation among the CD68 fractions (cd1, cd2, cd3) and flow-through fractions (ft1, ft2, ft3) belonging to three paired replicates. (D) Of the 1671 proteins identified, 28.2% were significantly enriched and 33.7% were significantly lower in the CD68 fractions relative to the flow-through (red circles, $p < 0.05$). Plotted as $-\log_{10}$ p-value (y axis) versus the $\log_2$ fold-change (x axis) of the protein abundance averaged between replicates with a false discovery of <0.1. Some significantly expressed proteins annotated are in blue dots.

and eosin (H&E) or the macrophage marker CD68 (Figure 1A, yellow border). Using the AutoSTOMP software module, the scar region was tiled into individual fields of view with defined pixel coordinates (Figure 1B). Field of view segmentation and the accuracy of the automated reimaging program were validated experimentally (Figure S1).

To biotinylate the CD68$^+$ SOI proteins within the scar borders, each tile was imaged at 488 nm (Figure 1B). Each image of the CD68 signal was thresholded, and the pixel coordinates were defined in an MAP file. The MAP file then guided the two-photon at a 720 nm wavelength, which selectively conjugated biotin-BP to proteins within the CD68$^+$ region. This process was fully automated across each field of view in the scar region tile array (Figure 1B). To validate the accuracy of biotin-BP targeting to the CD68$^+$ regions, some sections were washed, stained with streptavidin-594, and reimaged (Figure 1C; note the photobleaching of post-STOMP CD68 signal). These data indicate that AutoSTOMP software allows the user to define regions of a tissue section, tile this region into fields of view, and accurately image and biotinylate SOI in an automated fashion.

AutoSTOMP Enriches Macrophage Endolysosomal and Inflammatory Signaling Proteins in CD68$^+$ Regions of Cardiac Infarcts

To enrich the CD68 SOI proteins, excess unconjugated biotin-BP was washed off of the slide, and a sample lysate was prepared. Biotinylated SOI proteins were streptavidin-precipitated, eluted as the "CD68" fraction. To measure protein levels of the rest part of the entire scar sample, the unbound, flow-through fractions were also collected (Figure 2A). Of note, the flow-through fractions are expected to contain CD68$^-$ regions, as well as any CD68$^+$ regions of the section that were deeper than the focal excitation volume of the two-photon (approximately 2.4 μm in the Z axis at 25×

https://doi.org/10.1021/acs.jproteome.1c00505
J. Proteome Res. 2021, 20, 4543−4552

magnification[17]). Peptides were identified by LC−MS/MS and MaxQuant LFQ[18] method, which measures the peak volume normalized across samples to limit artifacts of run-to-run variability on the LC−MS.

A total of 1671 rat proteins were identified across the CD68 and flow-through replicates. Relative expression of each protein across the samples was evaluated by *z*-score and hierarchical clustering, which indicated that the majority of proteins identified were enriched in CD68 (Figure 2B, left green bar) or lower in CD68 fractions (Figure 2B, left red bar) relative to flow-through fractions. T-distributed stochastic neighborhood embedding (t-SNE)[15] supported the conclusion that AutoSTOMP effectively enriched SOI proteins as there was more similarity within fractions than within each sample (Figure 2C).

Of the 1671 proteins identified, 28.2% of proteins were more abundant in the CD68 fractions and 33.7% of proteins were less abundant compared to the flow-through fractions (Figure 2D, red dots FDR < 0.1). As expected, macrophage markers CD68 (used to guide tagging), lysozyme 2 (LYZ2 or LYZM), and lysophosphatidylcholine acyltransferase 2 (LPCAT2) were enriched in the CD68 fractions (Figure 2D).[19−21] The LYZ2 signal is colocalized with CD68 (Figure 3A). Consistent with

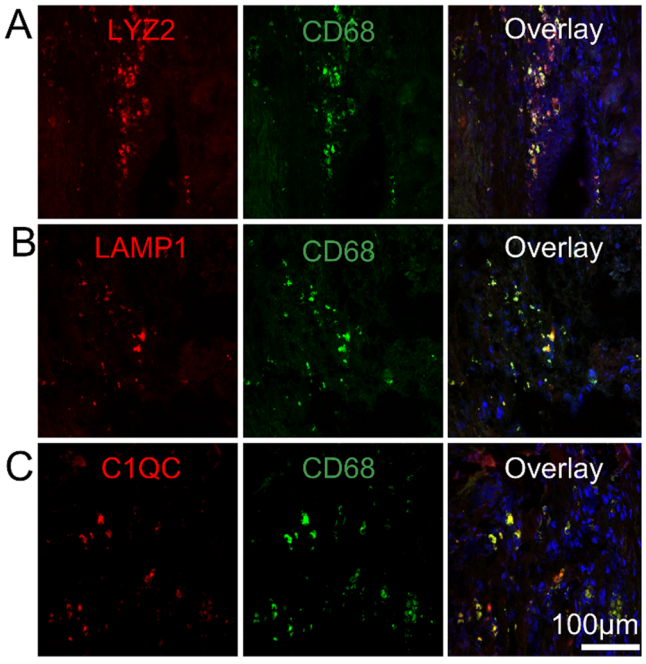

Figure 3. CD68$^+$ macrophage partially colocalizes with LYZ2, LAMP1, and C1QC in rat cardiac infarcts. One week rat cardiac infarcts were stained for CD68 (green) as described in Figure 1 and antibodies specific to the macrophage marker LYZ2 (A, red), the lysosomal protein LAMP1 (B, red), and the complement protein C1QC (C, red). Samples were counterstained with DAPI. $N = 3$.

the large phagocytic capacity of macrophages, the lysosomal proteins, lysosome-associated membrane glycoprotein 1 (LAMP1), acid phosphatase 2 (ACP2), vacuolar adenosine triphosphate (ATP)-dependent proton pumps (ATP6V1B2, ATP6V1C1, ATP6V1H), and cathepsin (CTSB, CTSZ) were enriched in CD68 fractions (Figure 2D). The CD68$^+$ signal is partially colocalized with LAMP1 (Figure 3B). The complement proteins C4 and C1Q, which are synthesized by macrophages in response to inflammatory stimuli and modulate phagocytic uptake of cargo, were enriched in CD68 fractions (Figure 2D).[22] C1QC is expressed by cardiac resident macrophage and colocalized with CD68 (Figure 3C).[23]

To identify broader signaling networks associated with CD68$^+$ macrophages, the proteins that were significantly different between the CD68 and flow-through fractions (Figure 2D, red) were analyzed using David Bioinformatic Resources to annotate gene ontology (GO) terms (Figure S2).[24] Consistent with inflammatory tissue remodeling, proteins involved in type 1 interferon cytokine signaling and glycerol 3-phosphate signaling and metabolism, a pathway that generates lipid signaling mediators of wound healing, were among the most represented "biological process" GO terms in CD68 fractions (Figure S2A). Proteins regulating amino acid metabolism (aspartate, glutamate), ammonium compound (carnitine), RNA export,[25] and extracellular matrix synthesis were enriched in flow-through fractions, consistent with muscle regenerative functions of stromal cells (Figure S2B). The central regulator of carnitine metabolism, acyl-coA dehydrogenase (ACADL) was one of the most significantly enriched proteins in the flow-through (Figure 2D). Extracellular matrix proteins included collagens (COL1A1 and COL18A1), fibronectin 1 (FN1), periostin (POSTN), and elastin microfibril interfacer 1 (EMILIN1), which are also enriched (Figure 2D).

Gene set enrichment analysis (GSEA) was also performed on all 1671 proteins using the REACTOME database (Figure S3).[26,27] The most highly enriched gene sets in the CD68 fractions were components of the Eph-ephrin and Fcγ receptor pathways, which signal through Rho GTPases (e.g., RhoA, Rac1, and Cdc42) to facilitate actin remodeling and the phagocytic uptake of cargo (Figure S3, red).[28−30] Interleukin 12 (IL-12), the main macrophage product necessary for IFN-γ expression, was also enriched in CD68 fractions (Figure S3, red).[31,32] Similar to the results of the GO search, the flow-through fractions were enriched for proteins belonging to mitochondrial biogenesis and respiration, muscle contraction, and extracellular matrix regulation (Figure S3, blue). In summary, these data show that AutoSTOMP is an effective tool to enrich and measure macrophage proteins in infarcted cardiac tissue sections.

AutoSTOMP Enriches Granulocyte Proteins, Eicosanoid Inflammatory Mediators, and Glycolytic Metabolism Machinery from IgG4$^+$ Inflammatory Lesions in Esophageal Biopsies

We next asked if AutoSTOMP could selectively enrich proteins associated with discrete regions of human tissue biopsies. Eosinophilic esophagitis (EoE) is a disease driven by dietary allergens that leads to focal inflammatory lesions within the esophagus, which are characterized by infiltration of eosinophils and mast cells and increased levels of Th2 cytokines.[33] The immunoglobulin G isotype IgG4 has recently been identified in the esophageal tissue and is increasingly recognized as a relevant feature of this disease.[34,35] However, progress toward understanding disease pathogenesis has been hindered by a lack of well-established animal models or the extremely limited access to samples from the primary site of inflammation and heterogeneity in the biopsy tissue.[36] To determine if AutoSTOMP was amenable to study EoE pathology, six 1 mm esophagus biopsies were isolated by endoscopy from a patient diagnosed with active EoE (Figure

https://doi.org/10.1021/acs.jproteome.1c00505
J. Proteome Res. 2021, 20, 4543−4552

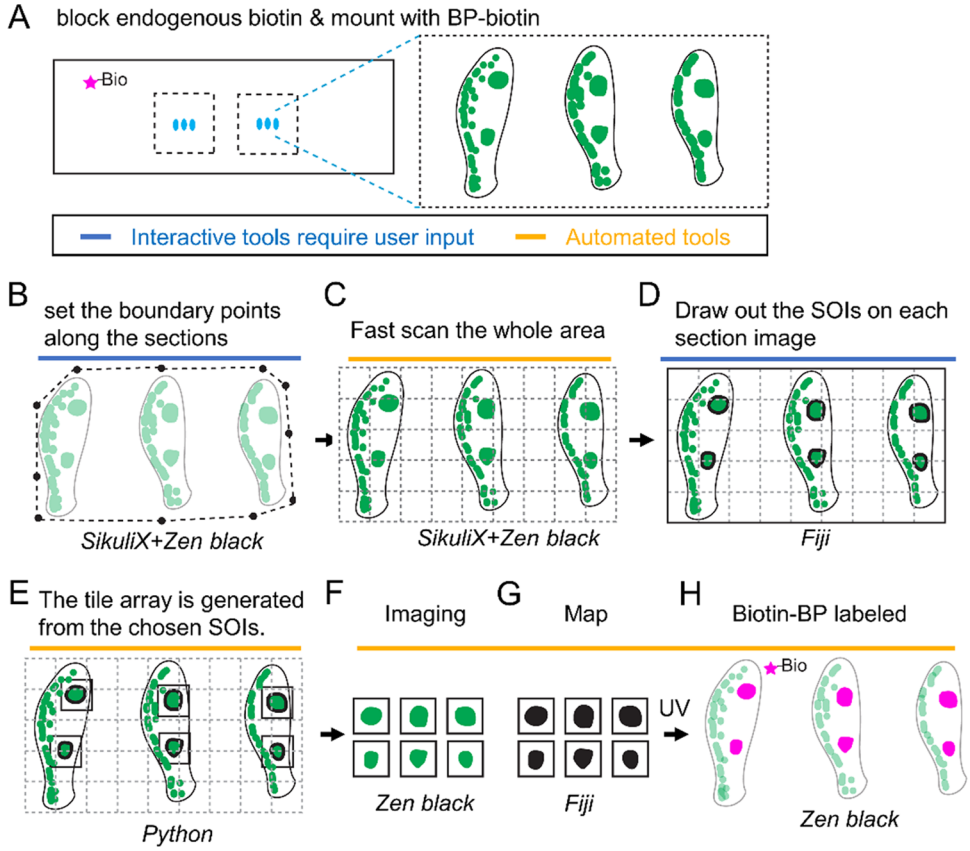

Figure 4. Schematic of AutoSTOMP-mediated targeting of discrete IgG4$^+$ lesions across multiple esophageal biopsy sections. 1 mm esophagus punch biopsies are isolated from a patient with active eosinophilic esophagitis (EoE). (A) 6−8 sections per slide are stained for IgG4 (green), and endogenous biotins are blocked and mounted with BP-biotin. A typical section contains five tiles at 340 μm × 340 μm per field of view using a 25× magnification objective lens. (B−H) SikuliX script allows the user to set the boundary points for all sections in Zen Black (B). (C) Boundary points then direct low-resolution tile scan in Zen Black. (D) IgG4$^+$ structures of interest (SOI) are identified by the user on each section in Fiji. (E) Python script maps the coordinates of each SOI to generate a tile array of SOI-containing fields of view. (F−H) SikuliX script automates SOI imaging in Zen black (F, green), MAP file generation in Fiji (G, black), and BP-biotin cross-linking in Zen Black (H, magenta), as described in Figure 1.

5). Immunofluorescence staining for lgG4 showed that the lesions measured between 50 and 300 μm in diameter or approximately 10% of each section (Figure 5A). Using AutoSTOMP, the boundary of all 6−8 sections per slide was defined by the user to facilitate a low-resolution tile scan (Figure 4A−C). To avoid the high background fluorescence signal from the apical epithelium, each lgG4$^+$ SOI was selected by the user (Figures 4D and 5B, "threshold" signal vs "MAP"). A tile array of the SOI pixel coordinates (Figure 4E) was then generated to automate biotin-BP tagging (Figure 4F−H). To validate biotin-BP targeting, some slides were reserved for streptavidin-594 staining and reimaged (Figure S4).

To identify the biotinylated proteins enriched in the lgG4$^+$ lesions (Figure 5A,B), the sample lysate was incubated with streptavidin beads (lgG4 fraction) and the unbound, flow-through fractions were reserved as a total protein control, as described in Figure 2A. In total, 2007 human proteins were identified across three samples, where each sample (1−3) represented paired lgG4 or flow-through fractions pooled from two biopsies (Figure 5C). When the level of each protein was evaluated across all samples, hierarchical clustering revealed three major groups enriched in IgG4 fractions (Figure 5C, left green bar) or enriched in flow-through fractions (Figure 5C, left red and blue bars). Variability in the flow-through samples accounted for the bimodal clustering of the red and blue groups. This indicated that the lgG4$^+$ regions were more similar in protein identity than the stromal cells from each biopsy pair and underscored the selective enrichment of the AutoSTOMP procedure. The selectivity of AutoSTOMP was also evaluated by t-SNE, which showed that despite the variability within flow-through fractions, there was more similarity within fractions than within each sample (Figure 5D).

Of the 2007 proteins identified in the patient's biopsies, 27.9% were significantly enriched in the lgG4 fractions and 12.3% were depleted in lgG4 fractions relative to the flow-through (Figure 5E). Granulocyte secretory proteins were among the most highly enriched proteins in the lgG4 fractions, including the proteoglycans PRG2 and PRG3, defensin DEFA3, and eosinophil peroxidase (EPX) (Figure 5E).[37] Enzymes regulating the synthesis of eicosanoid lipid inflammatory regulators were also enriched in the IgG4 fractions, including arachidonate-15 lipoxygenase (ALOX15), leukotriene A-4 hydrolase (LTA4H), and glutathione S-transferase P (GSTP1), which modifies prostaglandin A2 upstream of eicosanoid synthesis.[38−40] Mediators of inflammatory cytokine production were also enriched in the IgG4 regions, including the transcription factors signal transducer and activator of transcription 1 (STAT1) and STAT3, the interferon-induced effector MX1, complement protein C4A,

https://doi.org/10.1021/acs.jproteome.1c00505
J. Proteome Res. 2021, 20, 4543−4552

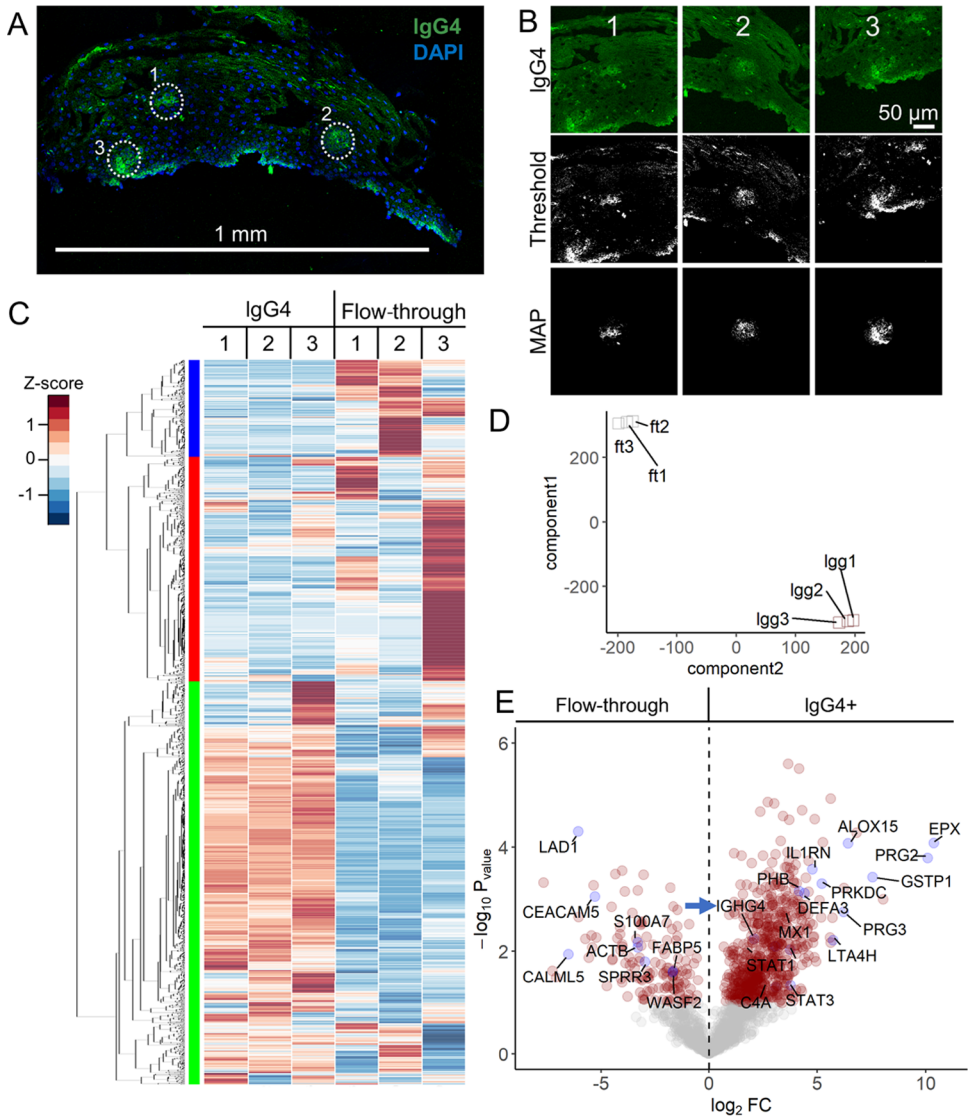

Figure 5. AutoSTOMP identifies eosinophil granule proteins associated with IgG4$^+$ lesions in EoE patient esophagus biopsies. (A) Representative section of an EoE patient biopsy stained with an antibody specific to lgG4 (green) and counterstained with DAPI (blue). IgG4$^+$ SOI are indicated by white dots, scale bar = 1 mm. (B) Three representative SOI tile images, thresholded images, and MAP files used to guide biotinylation of each SOI. (C, D) Biotinylated proteins, the "lgG4" fraction, or the unlabeled flow-through were isolated and identified as described in Figure 2A. Each sample represents sections pooled from two biopsies. (C) 2007 human proteins were identified and plotted by row z-score normalized across all of the samples. Hierarchical clustering (left) indicates three enrichment groups. (D) T-distributed stochastic neighborhood embedding (t-SNE) accounts for variation among the lgG4 fractions (lgg1, lgg2, lgg3) and flow-through fractions (ft1, ft2, ft3) across the three samples. (E) Of the 2007 proteins identified, 27.9% of proteins were significantly enriched and 12.3% of the proteins were significantly lower in the lgG4 fractions relative to the flow-through fractions (red circles, $p < 0.05$, FDR < 0.1). Plotted as $-\log_{10}$ p-value (y axis) versus the $\log_2$ fold-change (x axis) of the protein abundance averaged between replicates with a false discovery of <0.1. IgG4 positive control (IGHG4, blue arrow indicated) is noted. Some significantly expressed proteins annotated are in blue dots.

and the type I IL-1 receptor antagonist (IL-1RA) consistent with local activation of the inflammatory response. There was a partial overlap in the staining of PRG2, ALOX15, and IL-1RA with the IgG4 lesions, confirming their presence in the patient's EoE lesions as determined by LC−MS/MS (Figure 6).

To identify signaling networks associated with the IgG4+ lesions, we searched the significantly differentially expressed proteins (Figure 5E, red) against the "biological process" GO term library. Most of the enriched pathways were characterized by the abundance of proteasome components detected in the IgG4 lesions (Figure S5A, asterisks). Independent of this proteasome signature, glycolytic metabolic pathways were the most highly represented GO terms in the IgG4 fraction, consistent with metabolic demands needed to drive an inflammatory response (Figure S5, red).[41] By contrast, the flow-through fractions were enriched in proteins regulating epithelial turnover and differentiation (Figure S5, blue) including fatty acid binding protein (FABP5), calmodulin-like 5 (CALML5), small proline-rich protein 3 (SPRR3), the calcium binding defensin S100A7, β-actin (ACTB), and Wiskott−Aldrich syndrome protein family member 2 (WASF2) (Figure 5E).[42] Although future studies with an expanded number of patients will be needed to draw definitive conclusions about the mediators of EoE, these data indicate that AutoSTOMP is an effective protein discovery tool to

https://doi.org/10.1021/acs.jproteome.1c00505
J. Proteome Res. 2021, 20, 4543−4552

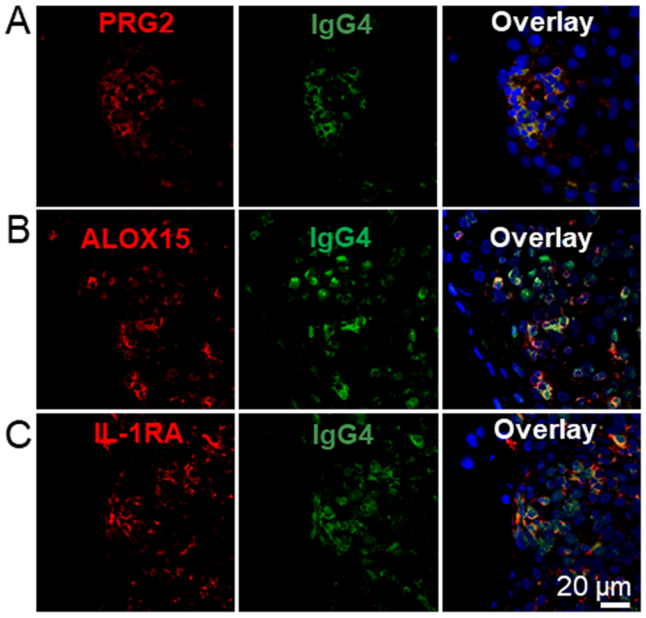

Figure 6. IgG4+ EoE lesions partially colocalize with inflammatory markers. EoE patient biopsy sections were stained for IgG4 (green) as described in Figure 5 and antibodies specific to the proteins PRG2 (A, red), ALOX15 (B, red), and IL-1RA (C, red). Samples were counterstained with DAPI. $N = 3$.

identify immune effectors from discrete inflammatory foci in human tissue biopsies.

CONCLUSIONS

This work meets a long-standing need for spatial proteomics tools that can be applied to discover mechanisms of human diseases. Our work is impactful in four areas. First, we present two novel, automated image parsing, and biotinylation strategies. Second, we report two new biochemical purification protocols for highly modified samples. Third, we have applied a label-free quantification methodology to normalize protein expression across samples. Finally, we report a direct translational application to primary human patient biopsies.

In theory, image-guided tagging means that almost any structure that can be visualized is a potential target for AutoSTOMP. However, in practice, heterogeneity in SOI size, shape, and frequency were barriers to performing STOMP in tissues. This was complicated by the requirement to use multiple software platforms to tile array (python), acquire images (Zen Black), threshold images (FIJI), and perform cross-linking (Zen Black) for each field of view. The icon recognition software SikuliX overcomes these limitations by allowing the user to automate image capture, image processing, and tiling discrete SOI across a tissue section. In addition, SikuliX automation facilitates the experimental time line since AutoSTOMP-mediated biotinylation can take several days per replicate for rare structures with a high degree of complexity. This time frame is similar to what would be required to accumulate samples by laser capture microdissection (LCM).[1] The spatial resolution of AutoSTOMP (~1 μm) is better than that of LCM (~10 μm), affording cleaner margins. Although LCM has been used with single-cell RNA sequencing, most proteomics readouts require pooled materials, similar to AutoSTOMP.[5] In contrast, mass spectrometry imaging (MSI) can be performed on cells or clusters of cells as small as 10−50 μm without pooling so that finite spatial information is retained.[2] However, use of MALDI as a readout means that protein detection is more limited by MSI.[2] In pooling individual structures for protein identification by LC−MS/MS analysis, AutoSTOMP affords detection of a wider range of proteins and quantification of their relative expression. This comes at the cost of loss of spatial resolution for individual cells; however, as discussed below, this can be compensated for by selecting colocalization criteria and repeating the AutoSTOMP experiment. All three of these techniques will likely prove particularly powerful when paired with new tools for multiparameter imaging such as imaging mass cytometry,[43] multiplexed ion bean imaging (MIBI),[44] or CHIP cytometry[45] that will facilitate validation of protein expression across cell types in heterogeneous tissues.

One benefit of AutoSTOMP is that it is performed on fixed samples. This facilitates banking of samples that can be sectioned, stained, and processed at later dates. This flow-through also means that, as new structural markers are identified by AutoSTOMP, the map file can be refined in subsequent experiments using new colocalization markers. However, fixation also introduces challenges for tissue digestions and streptavidin precipitation. The cardiac infarct model was specifically selected because extensive extracellular matrix is noted to be problematic for tissue digestion and protein purification. Here, we describe a hydroxylamine tissue lysis protocol that allows us to effectively enrich cellular proteins and ECM components for streptavidin precipitation and identification by LC−MS. Hydroxylamine interrupts protein quaternary structure by cleaving peptide bonds, in particular, at asparagine−glycine cites.[10] For tissues that require less stringent lysis procedures, like esophageal biopsy tissue, denaturation in DTT and SDS was sufficient to enrich granulocyte-specific proteins and immune signaling molecules associated with IgG4.

Finally, developing a protocol to analyze protein levels in the flow-through has maximized the use of each sample, which is important for rare samples or in studies where biopsy-to-biopsy variability is expected to be high. A central challenge in making this comparison is that protein abundance in the AutoSTOMP fraction is very low, typically less than or equal to 1 μg. By contrast, the protein abundance and diversity in the flow-through portion of the sample are typically far higher. For low abundance samples, normalizing protein levels across replicates is important to limit artifacts or run-to-run variability on the mass spectrometer. Isotopic postlabeling and sample pooling for a single LC−MS/MS run are one solution. However, this methodology would increase competition for detection of rare proteins in the AutoSTOMP sample relative to the flow-through fraction. To circumvent these problems, we employed a MaxQuant LFQ label-free quantification method that normalizes protein abundance across individual samples. This method has been validated to compare samples where protein abundance differs by 10-fold, which is well suited to address these data sets.[14,18] In summary, these data indicate that AutoSTOMP is a robust and flexible tool to perform protein discovery in heterogeneous tissues and primary tissue biopsies, with wide implications for our understanding of human disease pathophysiology.

https://doi.org/10.1021/acs.jproteome.1c00505
J. Proteome Res. 2021, 20, 4543−4552

■ ASSOCIATED CONTENT

Supporting Information

The Supporting Information is available free of charge at https://pubs.acs.org/doi/10.1021/acs.jproteome.1c00505.

AutoSTOMP accurately defines the coordinates of individual fields of view within user-defined borders and targets them for reimaging (Figure S1); inflammation regulatory pathways are enriched in CD68 fractions isolated by AutoSTOMP, and amino acid metabolism pathways are enriched in flow-through fractions of rat cardiac infarcts (Figure S2); phagosome maturation and inflammatory signaling pathways are enriched in the CD68 fractions, and mitochondrial metabolism pathways are enriched in the flow-through fractions of rat cardiac infarcts (Figure S3); AutoSTOMP selectively biotinylates IgG4+ regions of human EoE esophagus biopsies (Figure S4); glycolytic metabolism and inflammatory pathways are enriched in lgG4+ regions of EoE biopsies and protein regulators of epithelial differentiation enriched in the flow-through (Figure S5); the antibodies used on rat scar tissues (Table S1); and the antibodies used on EoE samples (Table S2) (PDF)

■ AUTHOR INFORMATION

Corresponding Author

Sarah E. Ewald − *Department of Microbiology, Immunology and Cancer Biology and the Carter Immunology Center, University of Virginia School of Medicine, Charlottesville, Virginia 22903, United States*; Email: se2s@virginia.edu

Authors

Bocheng Yin − *Department of Microbiology, Immunology and Cancer Biology and the Carter Immunology Center, University of Virginia School of Medicine, Charlottesville, Virginia 22903, United States*; orcid.org/0000-0003-1755-2728

Laura R. Caggiano − *Department of Biomedical Engineering, University of Virginia School of Medicine, Charlottesville, Virginia 22903, United States*

Rung-Chi Li − *Division of Allergy and Clinical Immunology, Department of Medicine, University of Virginia School of Medicine, Charlottesville, Virginia 22903, United States; Department of Allergy and Immunology, Northern Light Health, Bangor, Maine 04401, United States*

Emily McGowan − *Division of Allergy and Clinical Immunology, Department of Medicine, University of Virginia School of Medicine, Charlottesville, Virginia 22903, United States*

Jeffrey W. Holmes − *Department of Biomedical Engineering, University of Virginia School of Medicine, Charlottesville, Virginia 22903, United States; School of Engineering, University of Alabama at Birmingham, Birmingham, Alabama 35294, United States*

Complete contact information is available at: https://pubs.acs.org/10.1021/acs.jproteome.1c00505

Author Contributions

B.Y. and S.E.E. designed the experiments. L.C. and J.H. performed rat cardiac infarcts. R.L. and E.M. collected clinical specimens. B.Y. performed AutoSTOMP experiments and data analysis. B.Y. and S.E.E. prepared the manuscript.

Notes

The authors declare no competing financial interest.

■ ACKNOWLEDGMENTS

The authors thank Dr. Nicholas E. Sherman and Dr. Jeong-Jin Park for LC−MS/MS services at the W.M. Keck Biomedical Mass Spectrometry Laboratory. This work was supported by NIH R21AI156153, R35GM138381 (S.E.E.), AHA/Allen Institute 31315 (J.H. and S.E.E.), and start-up funds from the University of Virginia SOM and the Emily Couric Cancer Center.

■ REFERENCES

(1) Espina, V.; Wulfkuhle, J. D.; Calvert, V. S.; VanMeter, A.; Zhou, W.; Coukos, G.; Geho, D. H.; Petricoin, E. F.; Liotta, L. A. Laser-Capture Microdissection. *Nat. Protoc.* **2006**, *1*, 586−603.

(2) Buchberger, A. R.; DeLaney, K.; Johnson, J.; Li, L. Mass Spectrometry Imaging: A Review of Emerging Advancements and Future Insights. *Anal. Chem.* **2018**, *90*, No. 240.

(3) Ly, A.; Longuespée, R.; Casadonte, R.; Wandernoth, P.; Schwamborn, K.; Bollwein, C.; Marsching, C.; Kriegsmann, K.; Hopf, C.; Weichert, W.; Kriegsmann, J.; Schirmacher, P.; Kriegsmann, M.; Deininger, S.-O. Site-to-Site Reproducibility and Spatial Resolution in MALDI−MSI of Peptides from Formalin-Fixed Paraffin-Embedded Samples. *Proteomics: Clin. Appl.* **2019**, *13*, No. 1800029.

(4) Théron, L.; Centeno, D.; Coudy-Gandilhon, C.; Pujos-Guillot, E.; Astruc, T.; Rémond, D.; Barthelemy, J.-C.; Roche, F.; Feasson, L.; Hébraud, M.; Béchet, D.; Chambon, C. A Proof of Concept to Bridge the Gap between Mass Spectrometry Imaging, Protein Identification and Relative Quantitation: MSI~LC-MS/MS-LF. *Proteomes* **2016**, *4*, No. 32.

(5) Yin, B.; Mendez, R.; Zhao, X.-Y.; Rakhit, R.; Hsu, K.-L.; Ewald, S. E. Automated Spatially Targeted Optical Microproteomics (AutoSTOMP) to Determine Protein Complexity of Subcellular Structures. *Anal. Chem.* **2020**, *92*, 2005−2010.

(6) Chen, C.-L.; Perrimon, N. Proximity-Dependent Labeling Methods for Proteomic Profiling in Living Cells. *Wiley Interdiscip. Rev.: Dev. Biol.* **2017**, *6*, No. e272.

(7) Branon, T. C.; Bosch, J. A.; Sanchez, A. D.; Udeshi, N. D.; Svinkina, T.; Carr, S. A.; Feldman, J. L.; Perrimon, N.; Ting, A. Y. Efficient Proximity Labeling in Living Cells and Organisms with TurboID. *Nat. Biotechnol.* **2018**, *36*, 880−887.

(8) Trinkle-Mulcahy, L. Recent Advances in Proximity-Based Labeling Methods for Interactome Mapping [Version 1; Referees: 2 Approved]. *F1000Research* **2019**, *8*, No. 135.

(9) Bar, D. Z.; Atkatsh, K.; Tavarez, U.; Erdos, M. R.; Gruenbaum, Y.; Collins, F. S. Biotinylation by Antibody Recognition—a Method for Proximity Labeling. *Nat. Methods* **2017**, *15*, 127−133.

(10) Barrett, A. S.; Wither, M. J.; Hill, R. C.; Dzieciatkowska, M.; D'Alessandro, A.; Reisz, J. A.; Hansen, K. C. Hydroxylamine Chemical Digestion for Insoluble Extracellular Matrix Characterization. *J. Proteome Res.* **2017**, *16*, 4177−4184.

(11) Dellon, E. S.; Gonsalves, N.; Hirano, I.; Furuta, G. T.; Liacouras, C. A.; Katzka, D. A. ACG Clinical Guideline: Evidenced Based Approach to the Diagnosis and Management of Esophageal Eosinophilia and Eosinophilic Esophagitis (EoE). *Am. J. Gastroenterol.* **2013**, *108*, 679−692.

(12) Ostasiewicz, P.; Zielinska, D. F.; Mann, M.; Wisniewski, J. R. Proteome, Phosphoproteome, and N-Glycoproteome Are Quantitatively Preserved in Formalin-Fixed Paraffin-Embedded Tissue and Analyzable by High-Resolution Mass Spectrometry. *J. Proteome Res.* **2010**, *9*, 3688−3700.

(13) Wiśniewski, J. R. Proteomic Sample Preparation from Formalin Fixed and Paraffin Embedded Tissue. *J. Vis. Exp.* **2013**, *79*, No. 50589.

(14) Tyanova, S.; Temu, T.; Cox, J. The MaxQuant Computational Platform for Mass Spectrometry-Based Shotgun Proteomics. *Nat. Protoc.* **2016**, *11*, 2301−2319.
(15) van der Maaten, L.; Hinton, G. Visualizing Data Using T-SNE. *J. Mach. Learn. Res.* **2008**, *9*, 2579−2605.
(16) Tyanova, S.; Temu, T.; Sinitcyn, P.; Carlson, A.; Hein, M. Y.; Geiger, T.; Mann, M.; Cox, J. The Perseus Computational Platform for Comprehensive Analysis of (Prote)Omics Data. *Nat. Methods* **2016**, *13*, 731−740.
(17) Benninger, R. K. P.; Piston, D. W. Two-Photon Excitation Microscopy for the Study of Living Cells and Tissues. *Curr. Protoc. Cell Biol.* **2013**, *59*, No. 4.
(18) Cox, J.; Hein, M. Y.; Luber, C. A.; Paron, I.; Nagaraj, N.; Mann, M. Accurate Proteome-Wide Label-Free Quantification by Delayed Normalization and Maximal Peptide Ratio Extraction, Termed MaxLFQ. *Mol. Cell. Proteomics* **2014**, *13*, 2513−2526.
(19) Chistiakov, D. A.; Killingsworth, M. C.; Myasoedova, V. A.; Orekhov, A. N.; Bobryshev, Y. V. CD68/Macrosialin: Not Just a Histochemical Marker. *Lab. Invest.* **2017**, *97*, 4−13.
(20) Clausen, B. E.; Burkhardt, C.; Reith, W.; Renkawitz, R.; Förster, I. Conditional Gene Targeting in Macrophages and Granulocytes Using LysMcre Mice. *Transgenic Res.* **1999**, *8*, 265−277.
(21) Abate, W.; Alrammah, H.; Kiernan, M.; Tonks, A. J.; Jackson, S. K. Lysophosphatidylcholine Acyltransferase 2 (LPCAT2) Co-Localises with TLR4 and Regulates Macrophage Inflammatory Gene Expression in Response to LPS. *Sci. Rep.* **2020**, *10*, No. 10355.
(22) Lubbers, R.; van Essen, M. F.; van Kooten, C.; Trouw, L. A. Production of Complement Components by Cells of the Immune System. *Clin. Exp. Immunol.* **2017**, *188*, 183−194.
(23) Dick, S. A.; Macklin, J. A.; Nejat, S.; Momen, A.; Clemente-Casares, X.; Althagafi, M. G.; Chen, J.; Kantores, C.; Hosseinzadeh, S.; Aronoff, L.; Wong, A.; Zaman, R.; Barbu, I.; Besla, R.; Lavine, K. J.; Razani, B.; Ginhoux, F.; Husain, M.; Cybulsky, M. I.; Robbins, C. S.; Epelman, S. Self-Renewing Resident Cardiac Macrophages Limit Adverse Remodeling Following Myocardial Infarction. *Nat. Immunol.* **2019**, *20*, 29−39.
(24) Huang, D. W.; Sherman, B. T.; Lempicki, R. A. Systematic and Integrative Analysis of Large Gene Lists Using DAVID Bioinformatics Resources. *Nat. Protoc.* **2009**, *4*, 44−57.
(25) Burnap, S. A.; Mayr, M. Extracellular Vesicle Crosstalk between the Myocardium and Immune System upon Infarction. In *Circulation Research*; Lippincott Williams and Wilkins, 2018; pp 15−17.
(26) Subramanian, A.; Tamayo, P.; Mootha, V. K.; Mukherjee, S.; Ebert, B. L.; Gillette, M. A.; Paulovich, A.; Pomeroy, S. L.; Golub, T. R.; Lander, E. S.; Mesirov, J. P. Gene Set Enrichment Analysis: A Knowledge-Based Approach for Interpreting Genome-Wide Expression Profiles. *Proc. Natl. Acad. Sci. U.S.A.* **2005**, *102*, 15545−15550.
(27) Fabregat, A.; Sidiropoulos, K.; Viteri, G.; Marin-Garcia, P.; Ping, P.; Stein, L.; D'Eustachio, P.; Hermjakob, H. Reactome Diagram Viewer: Data Structures and Strategies to Boost Performance. *Bioinformatics* **2018**, *34*, 1208−1214.
(28) Darling, T. K.; Lamb, T. J. Emerging Roles for Eph Receptors and Ephrin Ligands in Immunity. *Front. Immunol.* **2019**, *10*, No. 1473.
(29) Massol, P.; Montcourrier, P.; Guillemot, J. C.; Chavrier, P. Fc Receptor-Mediated Phagocytosis Requires CDC42 and Rac1. *EMBO J.* **1998**, *17*, 6219−6229.
(30) Hanna, S. J.; McCoy-Simandle, K.; Miskolci, V.; Guo, P.; Cammer, M.; Hodgson, L.; Cox, D. The Role of Rho-GTPases and Actin Polymerization during Macrophage Tunneling Nanotube Biogenesis. *Sci. Rep.* **2017**, *7*, No. 8547.
(31) Eriksson, U.; Kurrer, M. O.; Sebald, W.; Brombacher, F.; Kopf, M. Dual Role of the IL-12/IFN-γ Axis in the Development of Autoimmune Myocarditis: Induction by IL-12 and Protection by IFN-γ. *J. Immunol.* **2001**, *167*, 5464−5469.
(32) Tait Wojno, E. D.; Hunter, C. A.; Stumhofer, J. S. The Immunobiology of the Interleukin-12 Family: Room for Discovery. *Immunity* **2019**, *50*, 851−870.
(33) O'Shea, K. M.; Aceves, S. S.; Dellon, E. S.; Gupta, S. K.; Spergel, J. M.; Furuta, G. T.; Rothenberg, M. E. Pathophysiology of Eosinophilic Esophagitis. *Gastroenterology* **2018**, *154*, 333−345.
(34) Clayton, F.; Fang, J. C.; Gleich, G. J.; Lucendo, A. J.; Olalla, J. M.; Vinson, L. A.; Lowichik, A.; Chen, X.; Emerson, L.; Cox, K.; O'Gorman, M. A.; Peterson, K. A. Eosinophilic Esophagitis in Adults Is Associated with IgG4 and Not Mediated by IgE. *Gastroenterology* **2014**, *147*, 602−609.
(35) Schuyler, A. J.; Wilson, J. M.; Tripathi, A.; Commins, S. P.; Ogbogu, P. U.; Kruzsewski, P. G.; Barnes, B. H.; McGowan, E. C.; Workman, L. J.; Lidholm, J.; Rifas-Shiman, S. L.; Oken, E.; Gold, D. R.; Platts-Mills, T. A. E.; Erwin, E. A. Specific IgG(4) Antibodies to Cow's Milk Proteins in Pediatric Patients with Eosinophilic Esophagitis. *J. Allergy Clin. Immunol.* **2018**, *142*, 139−148.e12.
(36) Mishra, A. Significance of Mouse Models in Dissecting the Mechanism of Human Eosinophilic Gastrointestinal Diseases (EGID). *J. Gastroenterol. Hepatol. Res.* **2013**, *2*, 845−853.
(37) Acharya, K. R.; Ackerman, S. J. Eosinophil Granule Proteins: Form and Function. *J. Biol. Chem.* **2014**, *289*, 17406−17415.
(38) Spiteri, M. A.; Bianco, A.; Strange, R. C.; Fryer, A. A. Polymorphisms at the Glutathione S-Transferase, GSTP1 Locus: A Novel Mechanism for Susceptibility and Development of Atopic Airway Inflammation. *Allergy* **2000**, *55*, 15−20.
(39) Singh, N. K.; Rao, G. N. Emerging Role of 12/15-Lipoxygenase (ALOX15) in Human Pathologies. *Prog. Lipid Res.* **2019**, *73*, 28−45.
(40) Fourie, A. M. Modulation of Inflammatory Disease by Inhibitors of Leukotriene A4 Hydrolase. *Curr. Opin. Investig. Drugs* **2009**, *10*, 1173−1182.
(41) Soto-Heredero, G.; Gómez de Las Heras, M. M.; Gabandé-Rodríguez, E.; Oller, J.; Mittelbrunn, M. Glycolysis—a Key Player in the Inflammatory Response. *FEBS J.* **2020**, *287*, 3350−3369.
(42) Rosekrans, S. L.; Baan, B.; Muncan, V.; Van Den Brink, G. R. Esophageal Development and Epithelial Homeostasis. *Am. J. Physiol.: Gastrointest. Liver Physiol.* **2015**, *309*, G216−G228.
(43) Chang, Q.; Ornatsky, O. I.; Siddiqui, I.; Loboda, A.; Baranov, V. I.; Hedley, D. W. Imaging Mass Cytometry. *Cytometry, Part A* **2017**, *91*, 160−169.
(44) Ptacek, J.; Locke, D.; Finck, R.; Cvijic, M.-E.; Li, Z.; Tarolli, J. G.; Aksoy, M.; Sigal, Y.; Zhang, Y.; Newgren, M.; Finn, J. Multiplexed Ion Beam Imaging (MIBI) for Characterization of the Tumor Microenvironment across Tumor Types. *Lab. Investig.* **2020**, *100*, 1111−1123.
(45) Hümmert, M. W.; Alvermann, S.; Gingele, S.; Gross, C. C.; Wiendl, H.; Mirenska, A.; Hennig, C.; Stangel, M. Immunophenotyping of Cerebrospinal Fluid Cells by Chipcytometry. *J. Neuroinflammation* **2018**, *15*, No. 160.

https://doi.org/10.1021/acs.jproteome.1c00505
J. Proteome Res. 2021, 20, 4543−4552